Biol. Cybern. 89, 200–213 (2003)
DOI 10.1007/s00422-003-0426-6
© Springer-Verlag 2003

Biological Cybernetics

Effect of light on stochastic phase synchronization in the crayfish caudal photoreceptor

S. Bahar

Department of Neurological Surgery, Weill-Cornell Medical College, 525 East 68th Street, Box #99, New York, NY 10021, USA

Received: 18 February 2002 / Accepted: 13 May 2003 / Published online: 14 July 2003

Abstract. Phase synchronization between the firing of the crayfish caudal photoreceptor (CPR) and an applied periodic hydrodynamic stimulus is investigated. It is shown that the CPR firing synchronizes with a periodic stimulus over a range of frequencies corresponding to the known sensitivity range of the crayfish to hydrodynamic stimuli. This synchronization is quantified using previously developed measures of synchronization such as the synchronization index; multiple stimulus-response locking ratios occur in this system that are consistent with theoretical predictions based on the theory of synchronization of noisy oscillators. The maximal synchronization for various locking ratios is shifted to higher frequencies in the presence of light.

Previous work (Pei et al. 1996a) has shown that the SNR of an applied low-amplitude, periodic, mechanical stimulus obtained from a power spectrum from delta pulses fit to CPR firing times is enhanced in light. In the present work, it is shown that an increase in the synchronization index parallels the increase in signal-to-noise ratio. This suggests that an increase in synchronization between the CPR firing and the mechanical stimulus is the mechanism by which the stimulus SNR is enhanced under light conditions; these results agree with theoretical predictions (Neiman et al. 1999c).

Synchronization between the two photoreceptor cells is also investigated. It is found that while both cells synchronize their firing with a periodically applied stimulus, there is little, if any, statistically significant synchronization between the two photoreceptors. The mutual synchronization between the two CPRs is not affected by light. These results are consistent with previous experimental results indicating that there is no mutual excitation between the CPRs (Flood and Wilkens 1978); the results also indicate that the responses to hydrodynamic stimuli on the left side of the crayfish are relatively isolated from those on the right.

The possible role of synchronization for information processing by the crayfish is discussed.

Correspondence to: S. Bahar
(e-mail: ssb2001@med.cornell.edu,
Tel.: +1-212-7465535, Fax: +1-212-7465592)

1 Introduction

1.1 Motivation

Scientific interest in the synchronization of oscillating systems dates back to the 17th-century investigations of Christian Huygens (1673). Oscillations in biological systems, however, are notoriously variable. The study of synchronization of biological systems was facilitated by the pioneering work of Stratonovich (1967) in the synchronization of stochastic (“noisy”) oscillating systems. A crucial point is that synchronization, as defined here, means a *mutual entrainment of two independent oscillators*, each with its own highly variable natural frequency. This situation is critically different from simply measuring the response of a nonoscillating, noisy system to a periodic stimulus.

Many systems in biology are oscillatory – circadian rhythms, heart rate, neural firing, calcium oscillations, etc. But these oscillations do not follow the crisp periodicity a mathematician might hope for; they are inherently stochastic as well as oscillatory. Synchronization of these noisy biological systems may be critical for many processes, such as neural information processing. The work of Stratonovich put the theory of stochastic synchronization on a firm mathematical footing. This was later extended with studies of synchronization between the phases of noisy oscillators (Rosenblum et al. 1996, 2001; Neiman et al. 1999a; Pikovsky et al. 2001), studies of synchronization-like phenomena in coupled bistable systems (Neiman 1994), and other work (see Pikovsky et al. 2001 for review).

With a theory firmly in place, experimental observations of biological synchronization have begun to pour in over recent years. For example, Schäfer et al. (1998a,b) characterized the synchronization between

breathing and heartbeat. Tass et al. (1998) demonstrated increased synchronization between cortical firing and muscle activity in Parkinsonian patients. Neiman et al. (1999b, 2000) observed synchronization in the electrosensitive afferent neurons of the paddlefish.

One of the most critical aspects of synchronization in stochastic neural systems is that the inherent noise, or variability, in the system requires that synchronization be assessed by *statistical measures* (Neiman et al. 1999b, 2000). For example, the present paper is concerned specifically with stochastic entrainment between the phase of the oscillator and the phase of the stimulus. But because of the high variability in biological oscillators, actual phase entrainment will typically persist for only a few cycles at a time, and one must resort to statistical measures to quantify the synchronization.

Stochastic synchronization is fundamentally different from measurements of instantaneous spike timing precision (Bialek et al. 1991; Pei et al. 1996b; Hunter et al. 1998). The latter methods are essentially concerned with neural coincidence detection, whereas stochastic synchronization addresses the process of entrainment of a noisy neural oscillator by a periodic signal *over some period of time*. (A neural oscillator may be thought of as a neuron that integrates and fires more or less regularly in response to a steady input.)

A further motivation for using synchronization methods is that these techniques provide much more information than more traditional cross-spectral methods. Phase synchronization methods are not equivalent to cross-spectral techniques; in fact, they provide a much stronger measure than the cross correlation. As pointed out by Tass et al. (1998) and Rosenblum et al. (2001), if two systems synchronize, their signals are correlated; the reverse case does not hold. Synchronization allows one to follow two systems, or a system and a stimulus, as they remain entrained over a range of frequencies. Cross correlation and related measures do not contain information about the time-evolution of the phase difference between two signals, whereas this information is front and center in phase synchronization analysis. Synchronization measures, such as the synchronization index defined below, allow the identification of various frequency-locking regimes, information that is not contained in cross-spectral methods. By measuring synchronization, therefore, it is possible to obtain detailed information about the time variation of the entrainment between a stimulus and a response as well as the type of mode locking between the two signals and the behavior of their entrainment as the driving frequency is varied.

In this paper, the role of stochastic synchronization in signal transduction in the crayfish caudal photoreceptor is experimentally investigated.

1.2 Background

The crayfish possesses two light-sensitive neurons in its abdominal sixth ganglion (Welsh 1934; Kennedy 1958a,b; Kennedy 1963; Wilkens 1988), one of which is illustrated in Fig. 1. These photoreceptive cells (caudal photoreceptors, or CPRs) increase their firing rate (typically from ~5 Hz to ~30 Hz) when illuminated by direct light within the visible range (Bruno and Kennedy 1962). In addition to being *primary* light sensors, the CPRs are *secondary* interneurons in a mechanosensory pathway used for detecting small hydrodynamic motions; the crayfish can detect water motions as small as 20 nm (Plummer et al. 1986) and is thought to use this exquisite sensitivity for predator avoidance (Pei et al. 1996a). The mechanoreceptor neurons that synapse onto the photoreceptors are sensitive to hydrodynamic motions in the frequency range 2–20 Hz, which overlaps with the fin-beat and tail-beat frequencies of fish that typically prey on the crayfish (Bainbridge 1958; Bleckmann et al. 1991; Drucker and Jensen 1996a,b; Ellerby and Altringham 2001; Webb 2002). Thus sensitivity to small-amplitude signals in this frequency range is of great importance for the crayfish's survival, and the range of parameters studied here is of great behavioral relevance.

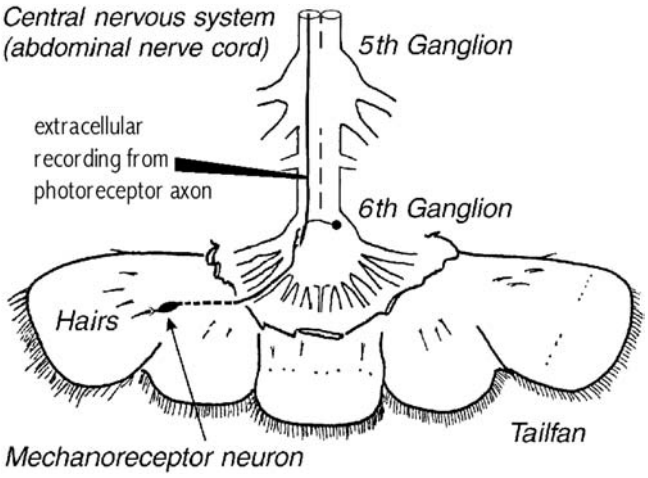

Fig. 1. Schematic diagram of the crayfish tailfan, showing the sixth and fifth abdominal ganglia. One of the two photoreceptors is shown in the sixth ganglion, with its axon extending upward toward the fifth ganglion. Note the position of the extracellular recording electrode in the connective between the sixth and fifth ganglia. It should be emphasized that this is a schematic diagram that greatly simplifies the complex interneural network in the ganglia. Only a few of the many mechanosensitive hairs on the surface of the tailfan are illustrated; in fact, there are hundreds of hairs on the telson and uropods. Note that the "fringe" hairs at the edge of the telson and uropods are not mechanosensitive. For more detailed illustrations of neural connectivity within the crayfish sixth ganglion, the reader is referred to the staining studies of Wilkens and Larimer (1972) and Simon and Edwards (1990)

Mechanosensory hairs on the crayfish tailfan are mechanically coupled to sensory neurons whose axons enter the sixth abdominal ganglion (Wilkens and Larimer 1972; Wiese 1976; Wiese et al. 1976; Wilkens 1988), as shown in Fig. 1. Many of these neurons synapse onto the CPR cells. Thus, recording extracellularly from the axons of one or both of the CPRs, the response to light or to periodic mechanical stimuli may be observed, depending on the experimental conditions (Flood and Wilkens 1978; Douglass and Wilkens 1998).

In addition to sharing a common pathway (the photoreceptor axon), these two sensory mechanisms – mechanosensitivity and light sensitivity – interact with one another. It has been known for some time that light affects mechanosensory sensitivity. Indeed, Welsh (1934) and later Edwards (1984) demonstrated that illumination of the CPRs can elicit behavioral responses such as backwards walking. Simon and Edwards (1990) showed that direct electrical stimulation of the CPRs leads to the same behavior.

Recently, however, Pei et al. (1996a) made a startling observation about the photoreceptor system: they demonstrated that **light enhances the encoding of weak periodic hydrodynamic stimuli**. The signal-to-noise ratio (SNR) of a low-amplitude periodic hydrodynamic stimulus (frequency 10 Hz, amplitude 147 nm peak-to-peak) calculated from a power spectrum generated from time series of photoreceptor spike times is enhanced as light levels are increased, up to a saturation level of $\sim$10 $\mu W/mm^2$. This has been interpreted as a stochastic resonance (Wiesenfeld and Moss 1995) effect in which added light increases the noise intensity in the input signal to the photoreceptor, leading to an enhancement of the SNR (Pei et al. 1996a).

The "stochastic resonance" effect described here was first illustrated in Pei et al. (1996a); however, the result is reproduced here, with data from crayfish used in this study, for completeness. Figure 2 shows power spectra from CPR recordings made in the dark (5 nW/mm^2, black trace) and in the light (22 $\mu W/mm^2$, dotted trace, extending off the *y*-scale). The hydrodynamic stimulus applied in both light and dark conditions has a peak-to-peak amplitude of 400 nm and a frequency of 10.5 Hz. Note the broad peak around 14–20 Hz in the light due to the light-induced increase in the CPR firing rate. This indicates the presence of a noisy intrinsic oscillator in the photoreceptor system, a prerequisite for synchronization of the form investigated here (see above). In this case, the SNR of the 10.5 Hz peak in the dark is 20.5, and in the light 51.7 (off scale).

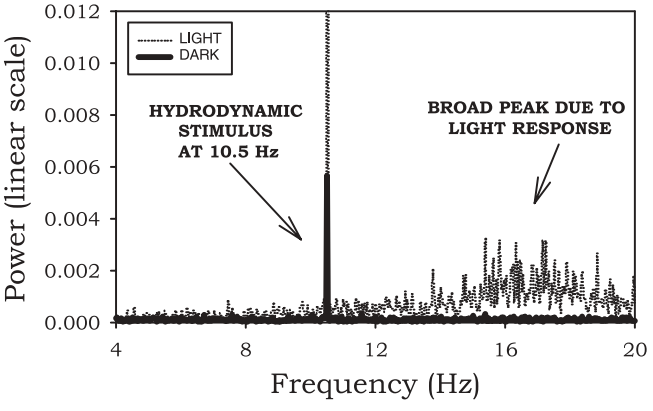

Fig. 2. Power spectra generated from delta pulses fit to a train of spike times recorded from the photoreceptor in dark (5 nW/mm^2) and light (22 $\mu W/mm^2$) conditions. The tailfan is driven with a sinusoidal hydrodynamic stimulus of amplitude 400 nm and frequency 10.5 Hz. A prominent peak can be seen at 10.5 Hz in the dark (*black trace*). In the light, the signal-to-noise ratio of this peak is increased threefold (see text). Note also the broad peak in the range 14–20 Hz due to the increased firing rate of the photoreceptor in the presence of light

In the present paper, the primary concern is to determine the *mechanism* by which the mechanosensory stimulus is encoded and how this encoding changes in the presence of light. In particular, is *phase synchronization* observed between the photoreceptor firing and a periodic (sinusoidal) mechanical stimulus? It is known that the direction in which the mechanosensory hairs are bent (and thus the phase of a mechanical stimulus) triggers the firing of the afferent neurons to which they are mechanically coupled (Wiese 1976; Wiese et al. 1976). Thus some phase relationship between the stimulus and response is to be expected. Indeed, recordings from the photoreceptor (Flood and Wilkens 1978) and other interneurons (Wiese 1976; Wiese et al. 1976) show well-defined clumps of neural spikes in what appears to be a fixed phase relationship with the stimulus.

But this is not sufficient to demonstrate synchronization. As Rosenblum et al. point out (2001; see also Pikovsky et al. 2001), synchronization is a dynamical process, not a state. This means that in order to demonstrate that the mechanosensory system encodes hydrodynamic signals by directly synchronizing with the stimulus frequency, it is necessary to demonstrate stochastic phase synchronization between the stimulus and response *over a range of frequencies*. Phase synchronization can be demonstrated (for example, by a synchronization index close to unity) for a time series at a fixed frequency. But under synchronization (whether stochastic or not), in its fullest sense, "if the frequency of one oscillator is slowly varied, the second system follows this variation" (Pikovsky et al. 2001). It is demonstrated below that this does indeed occur in the CPR system.

2 Methods

2.1 Experimental

In each experiment, the crayfish (*Procambarus clarkii*, Carolina Biological) tailfan and abdominal nerve cord below the second ganglion were dissected free of the abdomen, and the connective between the fifth and sixth ganglia was desheathed. Recordings were made with a suction micropipette filled with 150 mM KCl, recording extracellularly from the axon of one or both of the photoreceptors between the fifth and sixth ganglia. The preparation was kept in van Harreveld's standard crayfish saline solution (van Harreveld 1936) at room temperature. Voltage spikes were amplified and recorded using a CED 1401 interface (Cambridge Electronic Design). Spike 2 software (CED) was used to determine spike times from the recordings. The data acquisition rate was 16667 Hz (i.e., 0.06-msec timesteps). Note that at this sampling rate our maximum error in calculating the phase of a spike within a 2π stimulus cycle may be calculated as follows. At the maximum stimulus frequency, 30 Hz, there are 33 msec per cycle, giving a possible error of 0.06 msec/33 msec, which is equivalent to 0.18% of a 2π cycle. Thus, even at this high

frequency, the phase is measured with high accuracy at this sampling rate.

Light was applied to both photoreceptors simultaneously via a halogen bulb (DDL, 20 V, 160 W) passed through a light pipe, with the exit of the pipe approximately 7.5 cm from sixth ganglion. For variable light levels, neutral density filters (Oriel, Stamford, CT) were placed between the bulb and the light pipe. Light levels were determined using a photometer (Graseby Optronics 371 Optical Power Meter) placed as close as possible to the location of the photoreceptor in the preparation. The spectral sensitivity of the CPR has been shown to have a maximum at 500 nm (Bruno and Kennedy 1962); the tungsten-halogen bulb used in the present experiments has significant spectral output in this wavelength range. It should be noted, however, that the work of Bruno and Kennedy was performed in excised nerve cords that had been chilled in van Harreveld's solution overnight; in contrast, in this paper the tailfan and nerve cord are placed immediately after dissection into van Harreveld's solution at room temperature. I make the assumption that the overnight chilling in the experiments of Bruno and Kennedy does not significantly change the spectral response function of the CPRs; however, this remains to be experimentally demonstrated.

The CPR cells were positively identified as follows. Once a clear recording was obtained from a single axon in the 5–6 connective, the preparation was allowed to recover in the dark (5 nW/mm^2) for 5 min. A bright light (22 μW/mm^2) was then turned on briefly. If the firing rate of the axon increased significantly (e.g., from 5 Hz in the dark to 30 Hz in the light) and then slowed again once the light stimulus was removed, it was determined that a CPR axon had been located.

Mechanical stimuli were applied as described in Douglass and Wilkens (1998) and Wilkens and Douglass (1994) by rigidly fixing the tailfan in a vertical configuration by means of one pin through each of the two outer uropods to a moveable post within a room-temperature saline bath. The post, attached to an electromechanical vibration transducer (Pasco Scientific, Model SF-9324), could be moved up and down at various frequencies and amplitudes, generating relative motion between tailfan and saline solution. Due to slack in the nerve cord, there was negligible motion at the recording site. A laser Doppler vibrometer (Polytec) was used to calibrate the actual motions of the post to which the tailfan was fixed. Due to the rigid pinning between the tailfan and the post, I make the reasonable assumption that there is no phase delay between the motion of the post and the motion of the tailfan.

The preparation was placed within a Faraday cage mounted on a vibration-isolation table (Technical Manufacturing Corporation, *MICRO*-g). Experiments were performed at room temperature (~18–22 °C). In all experiments described below, unless otherwise indicated, "dark conditions" refers to a measured light level of 5 nW/mm^2, and "light conditions" refers to a measured value of 22 μW/mm^2.

2.2 Theoretical

If the neural firing times are denoted as t_k, $k = 0, 1, 2, \ldots, N$, and the upward zero-crossing times of the applied periodic stimulus as τ_i, $i = 0, 1, 2, \ldots, M$, then the phase difference of the kth spike with respect to the stimulus is

$$\phi(t_k) = 2\pi \frac{(t_k - \tau_i)}{\tau_{i+1} - \tau_i} \tag{1}$$

where $\tau_i < t_k < \tau_{i+1}$ (Neiman et al. 1999b; Rosenblum et al. 2001; Neiman et al. 2000; Pikovsky et al. 2001); $\phi(t_k)$ will have values between 0 and 2π. (A similar phase difference measure may be calculated between two different spiking neurons, where τ_i, instead of the zero-crossing times of the stimulus, represents the firing times of the second neuron.) The *continuous* phase of the neural firing, which can fall between 0 and infinity, rather than being "wrapped" modulo 2π, is defined at time t as

$$\phi(t) = 2\pi \frac{(t - t_i)}{t_{i+1} - t_i} + 2\pi i \tag{2}$$

where t_i is the time of the ith spike (Neiman et al. 1999b; Neiman et al. 2000; Rosenblum et al. 2001; Pikovsky et al. 2001).

If a neuron fires m times during n stimulus cycles, the $n : m$ phase-locking condition is

$$|n\phi(t) - m\phi_{\text{stim}}(t) - \delta| < \text{const.} \tag{3}$$

for the ideal case where there is no noise in the system. Here, $\phi(t)$ is the phase of the neural firing given in Eq. 2, $\phi_{\text{stim}}(t) = 2\pi f_o t$ is the continuous phase of the stimulus, and δ is the average phase shift between the two signals (Rosenblum et al. 2001). When condition Eq. 3 holds, the oscillator (neuron) and driving stimulus are said to be $n : m$ phase locked, and the $n : m$ phase difference is defined as

$$\Phi_{n,m}(t) = \left[2\pi \frac{(t - \tau_i)}{(\tau_{i+1} - \tau_i)} + 2\pi i\right] n - 2\pi m f_o t \tag{4}$$

It is important to note that the synchronization condition (Eq. 3) is fulfilled not just for a single set of system parameters but rather over a finite range (the synchronization region). A plot of parameters such as stimulus frequency and amplitude for which synchronization occurs often shows multiple synchronization regions, corresponding to different frequency lockings (i.e., different values of n and m). These plots are referred to as Arnol'd tongues (Moon 1992). The experimentally observed progression across 1:2, 1:1, and 2:1 locking patterns, discussed below, is an example of this phenomenon.

In a noisy system, the phase difference (Eq. 3) becomes unbounded, and we can speak of synchronization only in a statistical sense. In this case, phase locking occurs only during the brief intervals where $\phi(t)$ remains constant between phase slips (where, due to noise, ϕ(t) abruptly changes by $\pm 2\pi$). Even though phase locking

may only hold for brief periods of time in a noisy system, the quality of synchronization in a statistical sense may be found by plotting the probability density of the phase differences (Eq. 4). The intensity of the first Fourier mode of this distribution,

$$\gamma_{n,m}^2 = \left\langle \cos(\Phi_{n,m}(t)) \right\rangle^2 + \left\langle \sin(\Phi_{n,m}(t)) \right\rangle^2 \quad (5)$$

where $\left\langle \cos(\Phi_{n,m}(t)) \right\rangle^2$ and $\left\langle \sin(\Phi_{n,m}(t)) \right\rangle^2$ are time averages, defines the synchronization index $\gamma_{n,m}$, which varies from 0 to 1 and is indicative of the relative strength of $n : m$ mode locking (Rosenblum et al. 2001).

The circle map (see, for example, Neiman et al. 1995) serves as a canonical model of phase locking in a driven nonlinear system. The map is of the form

$$\phi_{n+1} = \phi_n + \rho - \frac{K}{2\pi}\sin(2\pi\phi_n) \quad (6)$$

modulo 1, where K determines the strength of the nonlinearity; the map can be considered as a nonlinear transformation of the phase of a driven oscillating system. The parameter ρ gives the ratio of the driving frequency to the response frequency in the unperturbed case (i.e., when $K = 0$). The system can be modified by adding a small amount of Gaussian white noise to the map, as

$$\phi_{n+1} = \phi_n + \rho - \frac{K}{2\pi}\sin(2\pi\phi_n) + \sqrt{2D}\xi_n \quad (7)$$

where ξ_n is Gaussian white noise and the parameter D controls the intensity of the noise term. Using the definition Eq. 5, the synchronization indices can be calculated analytically from the set of phases generated by the map (Eq. 7). The rotation number, defined as

$$rot = \lim_{n\to\infty} \frac{\phi_n - \phi_0}{n+1} \quad (8)$$

gives the actual ratio of the drive frequency to the response frequency and will be slightly different from ρ due to the presence of the nonlinear term.

A final point that should be mentioned here is the criteria sufficient to determine synchronization. An experimental setting where one cannot alter the coupling or frequencies of the oscillators whose synchronization one wishes to demonstrate is known as "passive" synchronization (Pikovsky et al. 2001). Here it may be necessary to perform a surrogate analysis (Dolan and Neiman 2002) to distinguish between the existence of coupling between the oscillators and simple coherence, which can exist even for linear combinations of signals. The case considered here, however, is that of "active" synchronization, where an oscillator is driven by a periodic stimulus whose frequency (or amplitude) can be controlled by the experimenter. In this case, synchronization can be demonstrated by tuning a drive parameter (in our case, frequency) and showing that synchronization persists over a range of drive parameter values. Nonetheless, we have performed statistical tests to demonstrate the difference between phase distributions in the synchronized and unsynchronized case, using a shuffled surrogate. This is discussed in more detail below.

3 Results

3.1 Frequency-detuning plots

The frequency-detuning plot is a standard demonstration of synchronization between a noisy oscillating system and a periodic driving force, showing the difference, or the ratio (used here), between the oscillator's average frequency and the driving frequency, plotted as a function of the driving frequency (Rosenblum et al. 2001; Pikovsky et al. 2001). A flat region in this curve is a signature of synchronization since it indicates that the drive and the response are frequency-locked over a range of frequencies. In other words, as the drive frequency is changed within this range, the response frequency follows along with it, maintaining a fixed numerical relationship to the drive. Figure 3 shows a frequency-detuning plot for a recording of neural spikes in the crayfish caudal photoreceptor. In the experiment shown in Fig. 3, a sinusoidal mechanical stimulus was applied at a range of driving frequencies f_o under dark conditions. Each stimulus was applied over a period of 2 min. Average photoreceptor firing frequency $\langle f \rangle$ was determined from the recorded spike times at each different stimulus frequency f_o. Figure 3 shows $f_o/\langle f \rangle$ vs. f_o, with two flat regions indicative of synchronization in the range 10–15 Hz, which corresponds to the range of maximum mechanical sensitivity of the photoreceptor response (Pei et al. 1996a).

The variability in the frequency-detuning plots is likely a result of intrinsic variability in the photoreceptor's firing. Frequency-detuning plots were recalculated using sets of spike times truncated to cover only 60 s of recording in order to determine whether nonstationarity in the data sets might cause variability in the flatness of the plateaus in the plot. No increase in "flatness" was observed in the frequency-detuning plateaus generated from the truncated data sets (not shown), indicating that nonstationarity over the recording period is not a significant source of variation. On the other hand, one might speculate that longer data sets, giving larger numbers of spikes over which to average in order to generate $\langle f \rangle$, might lead to increased smoothness in the

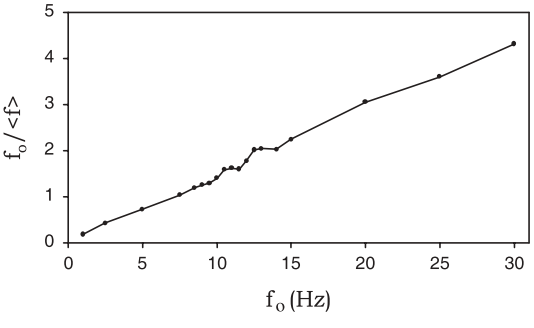

Fig. 3. Frequency-detuning curve under dark conditions (5 nW/mm^2). Tailfan was driven with a hydrodynamic stimulus of amplitude 400 nm over a range of frequencies (x-axis). The y-axis shows the ratio of the driving frequency over the average firing rate of the photoreceptor (recorded at each frequency for 2 min)

data. In order to test this, some experiments were performed using a recording time of 4 min rather than 2 min. No significant change in the "flatness" of the plateaus was observed in this case. (Longer periods of recording at each frequency were not used, since nonstationarity does become a problem in data records of this length under light conditions, as the photoreceptor accommodates the increased light level and the average firing rate undergoes a gradual decrease.)

Intrinsic variability in the average firing rate is not the only source of noise in the frequency-detuning plot. Due to the noisy nature of the neural firing, phase synchronization, as discussed above, is only maintained for short periods of time, interrupted by phase slips, where the phase difference between the neural firing and the stimulus changes by $\pm 2\pi$. Frequency entrainment, strictly speaking, only occurs over time periods where $\phi(t)$ is constant and is thus disrupted by each phase slip. Thus even at a single frequency f_o, frequency entrainment between the neuron and the periodic stimulus is maintained only for a few cycles at a time, punctuated by frequent phase slips, and it can be said that frequency-response lockings in this system exist in a statistical sense only. Luckily, however, more quantitative methods than the frequency-detuning plot exist for measuring the synchronization between the photoreceptor firing and the applied stimulus, as will be discussed in the next section.

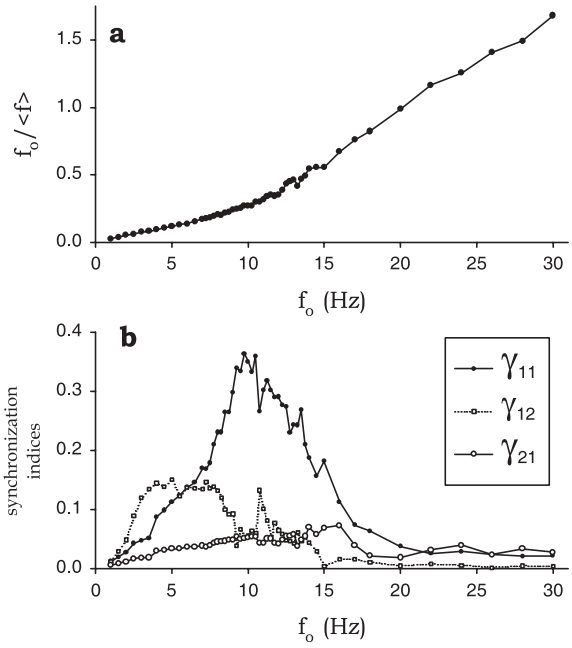

Fig. 4a,b. **a** Frequency-detuning curve under dark conditions using a stimulus amplitude of 6 μm. **b** Synchronization indices as defined in Eq. 4, γ_{12} (*open squares*), γ_{11} (*black circles*), and γ_{21} (*open circles*) calculated at each frequency shown in **a**. Recordings were made at each frequency for 4 min

3.2 Quantifying synchronization: experimental measures of the synchronization index

Figure 4a illustrates the frequency-detuning curve for a photoreceptor driven over various frequencies ranging from 1 to 30 Hz under dark conditions. Several flat regions are found between the frequencies 9 and 15 Hz. The synchronization index $\gamma_{n,m}$, defined in Eq. 5, may now be used to *quantify* this result. Figure 4b shows synchronization indices γ_{11} (filled circles), γ_{12} (open squares), and γ_{21} (open circles). Well-defined peaks are observed in γ_{11} and γ_{12} and a less well-defined peak in γ_{21}. Note that the largest peak, γ_{11}, occurs over the range where flat regions appear in the frequency-detuning curve.

Figure 4b also indicates that the different synchronization indices have maxima at different frequencies; γ_{12} has a peak at ~4.5 Hz, γ_{11} has a peak at ~9 Hz, and γ_{21}, though it has no sharp peak, has a maximal value at 16 Hz. This indicates that at low frequencies there is a region where on average two spikes occurs for every stimulus cycle (1:2 locking, corresponding to the maximum in γ_{12}). At higher frequencies, where γ_{11} is maximal, 1:1 locking is dominant, and 2:1 locking is observed at 14–16 Hz. The progression across 1:2, 1:1, and 2:1 locking patterns as one sweeps across a range of frequencies is typical of synchronization in nonlinear systems (i.e., Arnol'd tongues, see Moon 1992).

The observations shown in Fig. 4 are typical of our experiments. In measurements performed in the dark on eight crayfish driven over a range of frequencies (typically 1 to 30 Hz) with a hydrodynamic stimulus amplitude of 6 μm peak-to-peak, clear maxima in the synchronization indices were observed in all animals. In all cases, a progression from 1:2 to 1:1 to 2:1 locking was observed, except in one animal where only a progression from 1:1 to 2:1 was observed and another where only a progression from 1:2 to 1:1 was found. These results indicate that the region of 1:2 (2:1) locking was "off scale" due to the variation in frequency response from animal to animal, and thus that the frequency range over which this locking occurred in these two crayfish was not sampled.

In one crayfish, 3:1 and 4:1 locking patterns were observed in addition to 1:2, 1:1, and 2:1. The frequency-detuning curve from this animal is shown in Fig. 5a. In Figs. 5b, c, and d, 1:2, 1:1, and 2:1 locking occurred at low frequencies compared to Fig. 4. Since these lockings occurred at relatively low frequencies within the crayfish's range of sensitivity, the system can be observed to pass through 3:1 and 4:1 locking regions (Figs. 5e and f).

3.3 Does light increase the quality of synchronization?

The synchronization behavior shown in Figs. 4 and 5, in the dark, can now be compared with that in the light in order to address one of the fundamental questions posed at the outset: does the synchronization change when the system is moved from dark conditions to light? In four of the eight animals, the experiment was repeated in the light. In these four animals, a progression from 1:2 locking to 1:1 to 2:1 was observed, except in one animal,

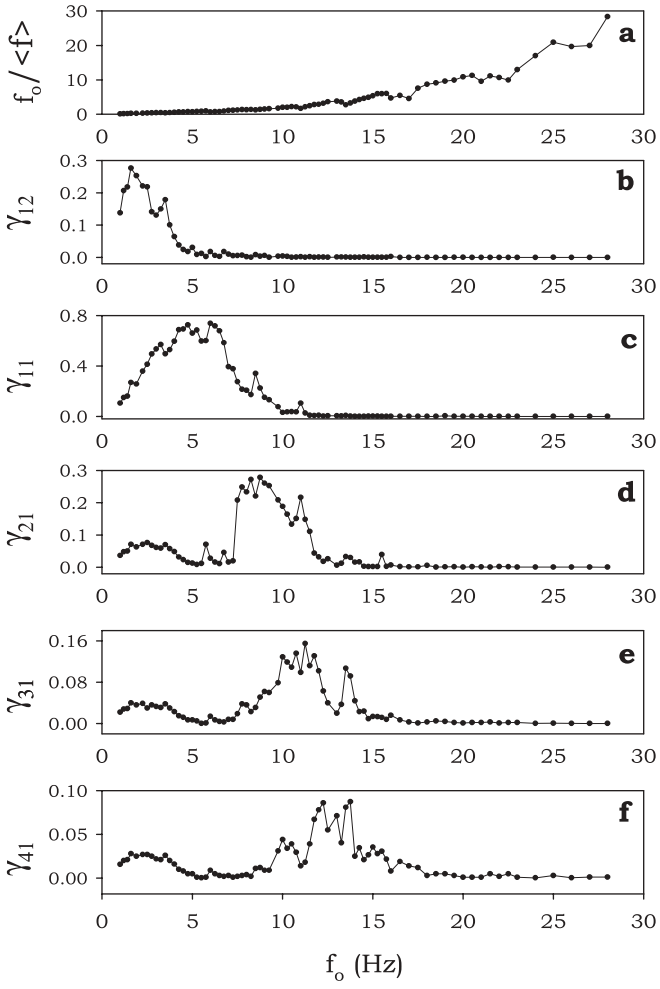

Fig. 5a–f. **a** Frequency-detuning curve under dark conditions using a stimulus amplitude of 6 μm. Recordings were taken for 2 min at each frequency. **b–f** Synchronization indices γ_{12}, γ_{11}, γ_{21}, γ_{31}, and γ_{41}

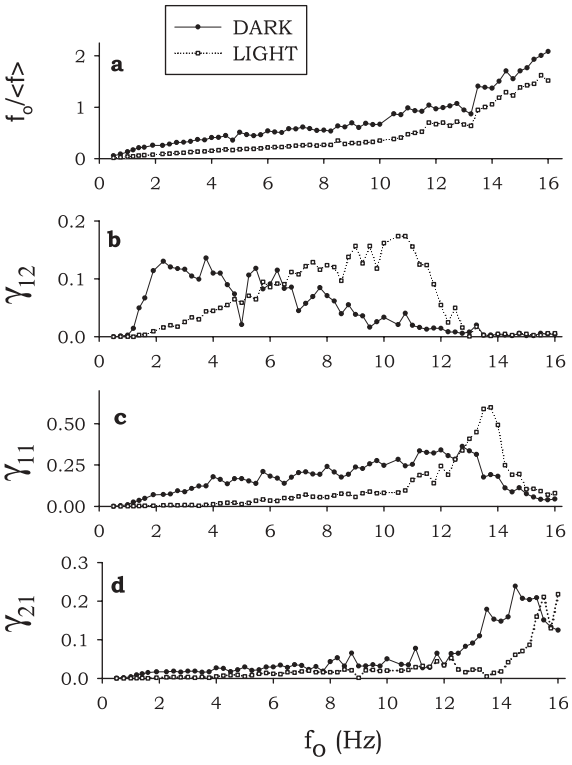

Fig. 6a–d. **a** Frequency-detuning curve under dark (5 nW/mm^2, *black circles*) and light (22 μW/mm^2, *open squares*) conditions. Recordings were made for 2 min at each frequency. Under light conditions, 5 min of rest were allowed in the dark (5 nW/mm^2) after each 2-min light recording. **b–d** Synchronization indices γ_{12}, γ_{11}, and γ_{21}, respectively, in dark (*black circles*) and light (*open squares*)

which showed only 1:2 and 1:1 locking. Further, if f_o^{nm} is defined as the frequency where γ_{nm} is maximized, in all cases f_o^{nm} (light) $> f_o^{nm}$ (dark) for each observed locking behavior.

Figure 6a shows frequency-detuning plots in dark (black circles) and light (open squares). In each case, the preparation was stimulated in the dark at the given driving frequency and amplitude 6 μm, and then the light was switched on. After allowing 30 s of accommodation to the increased light conditions, the stimulus protocol was repeated. At least 3 min of rest under dark conditions was allowed before moving to the next frequency. While noisier than the frequency-detuning curves in Figs. 3 and 4, a flat region is observed in both dark and light at ~11–13 Hz. This is a somewhat higher frequency range than the typical range of sensitivity for the crayfish (Plummer et al. 1986) and indicates the variability observed from one animal to the next in typical experiments (see discussion of Fig. 5). Figs. 6b, 6c, and 6d show γ_{12}, γ_{11}, and γ_{21}, respectively, with data for dark conditions shown by filled circles and in light shown by open squares. As before, the progression of maximal synchronization indices under dark conditions moves from γ_{12} (Fig. 6b) to γ_{11} (Fig. 6c) to γ_{21} (Fig. 6d). The γ_{21} peak is at the far right of panel 7d, at the edge of the measured frequency range, and indeed approaching a frequency range that may be out of the normal range of sensitivity of crustaceans altogether (Goodall et al. 1990; Popper et al. 2001), and certainly beyond the tail-beat and fin-beat frequency of most crayfish predators (Bainbridge 1958; Bleckmann et al. 1991; Drucker and Jensen 1996a,b; Ellerby and Altringham 2001; Webb 2002).

A similar progression of maxima is observed in the light (open squares) for γ_{12}, γ_{11}, and γ_{21}. In each case, f_o^{nm} (light) $> f_o^{nm}$ (dark). This suggests that the frequency response characteristics of the photoreceptor are shifted to higher frequencies in the light.

In one crayfish, the synchronization experiment was performed at amplitude 400 nm as well as at 6 μm. Results (see Table 1) were similar to those observed at the larger amplitude: peaks in γ_{12}, γ_{11}, and γ_{21} were observed in both dark and light conditions, with f_o^{nm} (light) $> f_o^{nm}$ (dark) for each index.

3.4 Effect of varying light levels on γ_{11} and SNR

In an experiment illustrated in Fig. 7, it is shown that γ_{11} increases as the light level is increased and passes

Table 1.

Expt. Number	Stimulus amplitude	Maximum γ_{12} dark	Maximum γ_{11} dark	Maximum γ_{21} dark	Maximum γ_{12} light	Maximum γ_{11} light	Maximum γ_{21} light
SB8a	6 μm	0.084	0.332	0.067	–	–	–
SB8b	6 μm	0.222	0.183	0.086	–	–	–
SB30	6 μm	0.344	0.186	0.034	0.280	0.180	0.013
SB31	6 μm	0.090	0.152	0.107	0.056	0.154	0.017
SB32a	6 μm	0.110	0.396	0.093	0.150	0.178	0.072
SB32b	400 nm	0.076	0.565	0.271	0.047	0.405	0.048
SB34	6 μm	0.151	0.364	0.073	–	–	–
SB35	6 μm	0.294	0.460	0.038	–	–	–
SB36	6 μm	0.136	0.363	0.239	0.175	0.599	0.218
SB37	6 μm	0.277	0.738	0.279	–	–	–
Avg (6 μm)		0.1784	0.3739	0.1287	0.1653	0.2778	0.0800
STDDEV (6 μm)		0.0982	0.1826	0.0958	0.0921	0.2145	0.0959
N (6 μm)		9	9	9	4	4	4

through a maximum. The figure shows the SNR plotted as a function of light level, given in $\mu W/mm^2$, in the top panel, and γ_{11} vs. light level in the bottom panel. The system was mechanically driven at 10 Hz and amplitude 2 μm for 2 min, then allowed to rest in the dark for at least 5 min before the application of a different light level. Error bars show standard deviations; $N = 4$ for highest and lowest light levels, and $N = 3$ for intermediate light levels. Figure 7 shows that the synchronization index shows a maximum at an intermediate value of light intensity (hypothesized to be related to the internal noise of the system); SNR passes through a maximum at the same light level. A maximal value of SNR as a function of noise is a signature of stochastic resonance effects (Wiesenfeld and Moss 1995). Recent theoretical studies suggest that an increase in synchronization measures paralleling an increase in the SNR should be observed in stochastic resonance as well (Neiman et al. 1998, 1999c). The observations shown in Fig. 7 are consistent with a stochastic resonance interpretation of the result shown in Fig. 2 and described in Pei et al. (1996a). These results are discussed in more detail in Bahar et al. (2002).

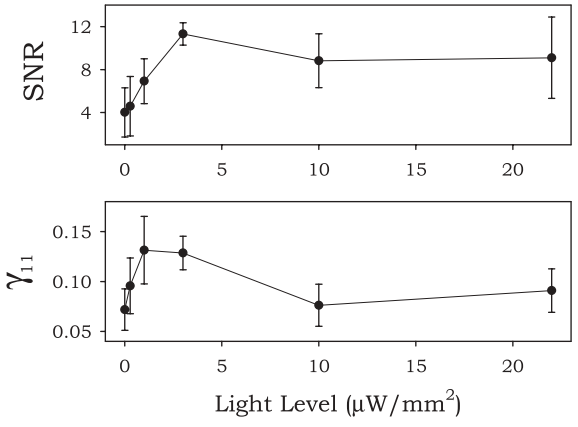

Fig. 7. a Signal-to-noise ratio at the driving frequency (10 Hz) for a photoreceptor driven with amplitude 2 μm at various light levels. *Error bars* represent standard deviations, $N = 4$ for largest and smallest light levels and $N = 3$ for intermediate light levels. **b** Synchronization index γ_{11} calculated for the same data sets. Five minutes of recovery time were allowed in the dark (5 nW/mm^2) after each recording under light conditions

3.5 Visualizing synchronization: phase difference histograms

The quantitative results described here may be complemented with the visual illustration of phase difference histograms. This graphic representation is based on the "wrapped" phase difference, modulo 2π, given in Eq. 1, with the τ_i's being the upward x-axis crossing times of the stimulus waveform. The phase difference between the photoreceptor firings and the stimulus can be plotted as a function of time (Figs. 8a and c) or binned into histograms (Figs. 8b and d). Figure 8 illustrates phase difference histograms corresponding to 10 Hz and 20 Hz in Fig. 4, recorded in the dark with a stimulus amplitude of 6 μm. At 10 Hz, γ_{11} is near its peak (see Fig. 4b), and a dark cluster of phase points is seen in Fig. 8a, which appears as a sharp peak in the histogram in 8b. In contrast, at 20 Hz, where γ_{11}, γ_{12}, and γ_{21} are all much smaller than their maximal values (Fig. 4b), and the phase difference between the CPR and the stimulus reflects this in the diffuse spread of values shown in Figs. 8c and d. Note also in Fig. 8a the lack of transient dynamics in the crayfish's response. There is no significant change in the synchronization index over time, i.e., the crayfish's "perception" of the stimulus is nearly instantaneous. Indeed, crayfish reaction times of <25 ms have been reported in the literature (Krasne and Lee 1988; Edwards et al. 1999; Steuer et al. 2001; Heberholtz et al. 2001).

In order to confirm that these distributions are statistically significantly different from random distributions, a Kolmogorov-Smirnov test (Sokal and Rohlf 1981) is used to compare each distribution with a set of phase differences generated from the same sets of data but randomly shuffled. The shuffling was performed by randomly scrambling the order of interspike intervals in each data set. This was performed for the data set in the top panels of Fig. 8. A comparison between Fig. 8b and the same data after shuffling indicates that there is

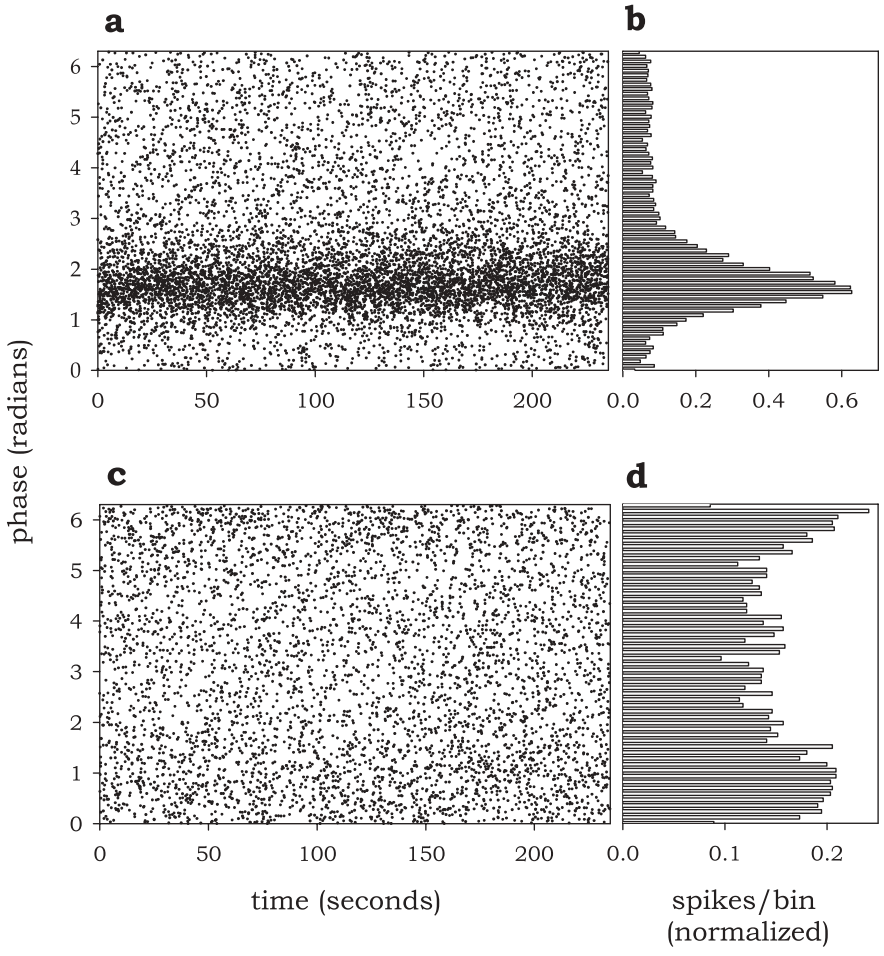

Fig. 8a–d. Phase difference calculated as in Eq. 1 as a function of time (**a**) with stimulation at a frequency of 10 Hz and amplitude of 6 μm (same data set as shown in Fig. 4 under dark conditions). Note the density of phase points around 1.5 rad. The probability density of phase distribution can be visualized more clearly when the phase points are binned into a histogram (**b**) (normalized to the total number of points in the sample); a sharp peak is clearly seen at ~1.5 rad. **c** Phase vs. time from the same experiment but at 20 Hz, where there is no significant synchronization. As discussed in the text, Kolmogorov-Smirnov tests show that both distributions are significantly different from control distributions obtained by randomly shuffling the interspike intervals in each data set

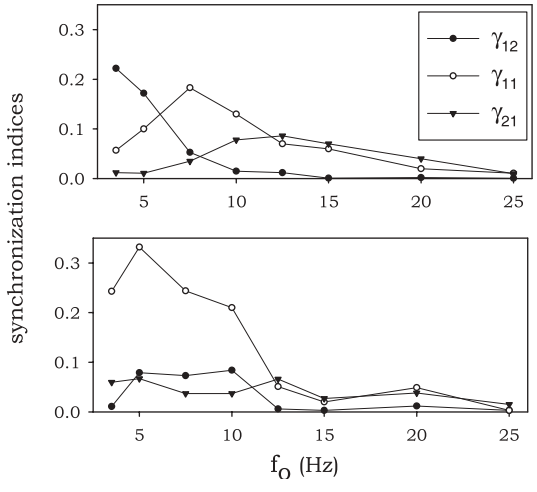

Fig. 9. Synchronization indices γ_{12}, γ_{11}, and γ_{21} as functions of driving frequency f_o for two photoreceptors (top and bottom panels, respectively) recorded simultaneously, using a driving amplitude of 6 μm under dark conditions. The spectrum of synchronization indices shows quite different behavior in one photoreceptor vs. the other

negligible probability of the two distributions arising from the same data set ($P_{Ho} < 0.0005$, where *Ho* is the null hypothesis). For the lower panels in Fig. 8, at 20 Hz, it is found that $P_{Ho} < 0.0005$ in the K-S test. Hence at both 10 Hz and 20 Hz the distribution of phases is statistically significantly different from a random distribution.

3.6 Mutual synchronization of the two photoreceptors

The two photoreceptors receive excitatory input from hairs on opposite sides of the crayfish tailfan. There is no evidence of excitatory connections between the two photoreceptors (Flood and Wilkens 1978). Nonetheless, ablation of nerve roots providing input to one photoreceptor has been shown to increase the response of the other CPR, indicating some possibly indirect (i.e., mediated by non-CPR interneurons) inhibitory effects between the two cells (Flood and Wilkens 1978). Given this observation and the fact that the two photoreceptors are coupled in the sense that they are subject to a common periodic mechanical stimulus, it can be asked whether the two photoreceptors (Eq. 1) respond similarly to a common stimulus and (Eq. 2) therefore synchronize with each other.

In order to address the first of these questions, Fig. 9 shows the synchronization indices γ_{12}, γ_{11}, and γ_{21} for both photoreceptors recorded simultaneously in a single crayfish stimulated with a 6-μm sine wave under dark conditions. The spectrum of synchronization indices shows quite different behavior in one photoreceptor vs.

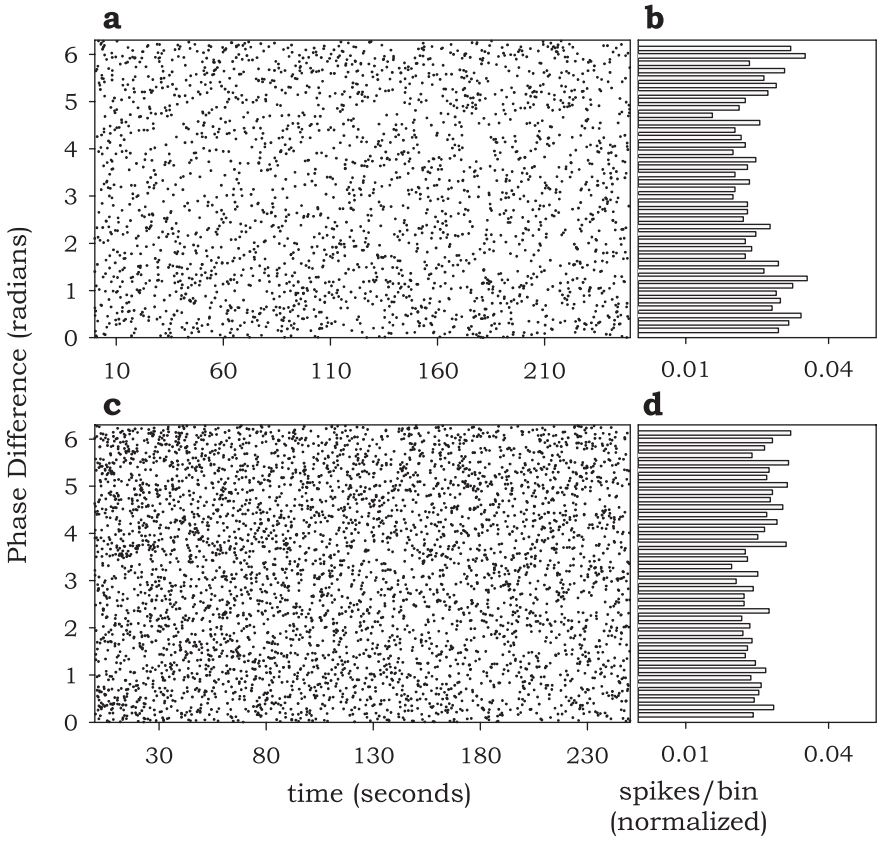

Fig. 10a–d. Phase difference between two photoreceptors as a function of time (**a, c**) and phase difference histograms (**b, d**) under dark (5 nW/mm^2) and light (22 μW/mm^2) conditions (top and bottom, respectively). Phase difference histograms are normalized to the total number of spikes in the sample. The preparation was driven with a hydrodynamic stimulus of frequency 10 Hz and amplitude 3 μm

the other. In one CPR (top panel), γ_{11} has a maximum at 7.5 Hz, while it is maximized at 5 Hz in the other CPR (lower panel). The CPR shown in the top panel also exhibits pronounced 1:2 locking at low frequencies, whereas the other CPR does not. These results indicate that the two photoreceptors have different frequency responses to the same signal. This may be at least partly explained by the fact that the two photoreceptors are often observed to differ by several Hertz in their intrinsic firing rates (recorded in the dark, with no applied stimulus), and entrainment by an applied stimulus likely depends in part on the frequency of the driven oscillator. The differential response may also reflect a decrease in sensitivity due to loss or damage to the motion-sensitive hairs on one side of the tailfan.

The top panels in Fig. 10 show phase differences between the two photoreceptors as functions of time and as histograms in dark (top panels) and light (bottom panels) conditions. Here the phase difference is calculated as in Eq. 1 with τ_i and t_k defined as the firing times of the two photoreceptors. While there are no well-defined peaks in the phase difference histograms (Figs. 11b and d), Kolmogorov-Smirnov tests show that in both cases there is a significant difference between each distribution and a control distribution generated by randomly shuffling each set of interspike intervals. In each case, $P_{Ho} < 0.0005$. Thus there appears to be some evidence for correlations between the two photoreceptors (compare, for example, the sharp peak in Fig. 8b). Application of light does *not* appear to significantly change the synchronization between the two photoreceptors. A K-S test between the phase difference histogram in the dark (Fig. 10b) and in the light (Fig. 10d) gives $P_{Ho} = 0.205$, indicating that there is a significant probability that the two distributions came from the same data set. The implications of this will be discussed below.

4 Discussion

4.1 Does light "improve" synchronization?

The results described here demonstrate that (1) stochastic synchronization occurs between the photoreceptor and the applied periodic stimulus and (2) the synchronization is changed, i.e., shifted to higher frequencies, in the presence of light. This brings us to the question of whether the quality of synchronization is *improved* in the light vs. the dark. The results show no overall increase in the maximal values of the synchronization indices in the light with respect to the dark. These results are shown in Table 1, which shows maximal synchronization indices for γ_{11}, γ_{12}, and γ_{21} for all eight crayfish studied. The first column lists an experiment label, the second the stimulus amplitude. (Experiments labeled "a" and "b" with identical stimulus amplitudes indicate dual recording from the two photoreceptors in one crayfish; thus data are compiled from nine CPRs over a total of eight animals.) The next six columns show maximum γs in

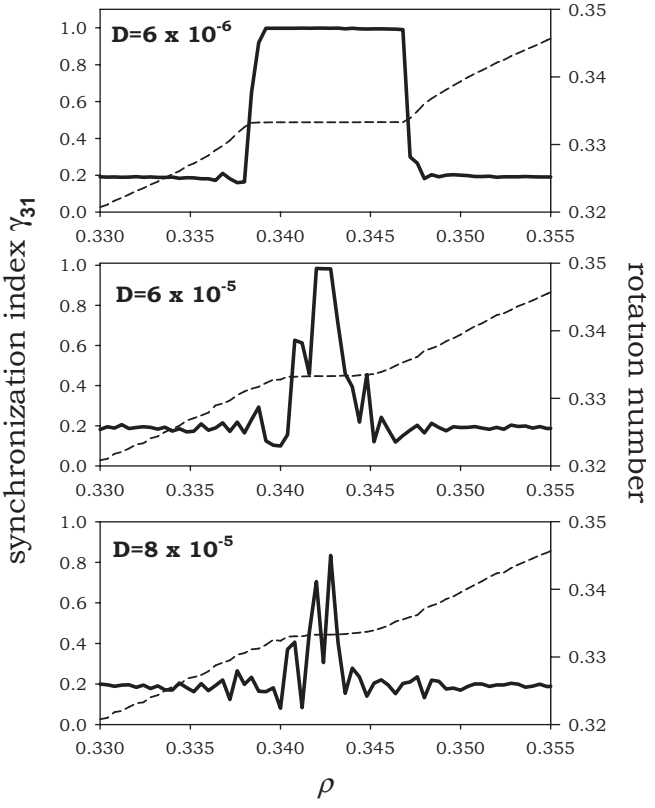

Fig. 11. Multiple peaks in the synchronization index γ_{13}, illustrated using the circle map. In each panel, $K = 0.665$. Rotation number is shown with a *dashed line*; the *solid line* shows γ_{13}. In the top panel, there is negligible added noise in the system ($D = 6 \times 10^{-6}$), in the middle panel $D = 6 \times 10^{-5}$, and in the bottom panel $D = 8 \times 10^{-5}$. At each value of ρ the circle map has been iterated 40,000 times, and the first 20,000 iterates are discarded as transients

dark and light. Average values are taken over the 6-μm measurements only, though the 400-nm values are included in the table for comparison. The average value of each synchronization index is larger in the dark than in the light, indicating that there is no *overall* increase in the quality of synchronization in the light. An unpaired t-test performed on all the 6 μm data indicates that there is no significant difference between the mean value of each synchronization index in the dark vs. the same index in the light. P-values for γ_{11}, γ_{12}, and γ_{21} are 0.678, 0.525, and 0.552 respectively.

While no overall increase in the quality of synchronization is observed, the synchronization index γ_{11} is found to increase in the light, with respect to the dark, *at specific frequencies* where an increase in signal-to-noise ratio (SNR) is observed. For example, for the data shown in Fig. 2, $\gamma_{11} = 0.140$ in the dark, and the index increases to $\gamma_{11} = 0.295$ in the light.

4.2 Sensitivity shifts to higher frequencies in the light

The shift in the synchronization index maxima to higher frequencies in the light (Fig. 6) indicates that the crayfish is sensitive to a higher frequency range in the light. This raises several questions whose answers may bear on fundamental problems of signal encoding. Is the higher-frequency range evolutionarily related to differences in the natural frequency range of environmental stimuli to which the crayfish is subject in the light, in contrast to lower-frequency stimuli it may be exposed to in the dark? Or is sensitivity to a higher frequency a dynamical result of signal encoding against a background of faster CPR firing in the light? This latter possibility can be tested using neural models where the firing rate can be realistically tuned over a 5–30-Hz range.

4.3 Secondary peaks in the synchronization index; circle map

In panels 5b–e, and in the γ_{12} curve in Fig. 4b, small secondary peaks in the synchronization index ride on the right edge of the main peak. While the data are certainly noisy, the repeated observation of this peaks warrants more than a dismissive glance. In fact, multiple peaks in a single synchronization index can be observed even in simple models of synchronization in the presence of noise. This effect is briefly illustrated here using the circle map model introduced in the Methods section. The rotation number (Eq. 8) expressed as a function of driving frequency is analogous to the frequency-detuning curve. Thus a peak in the synchronization index γ_{13} would be expected for rot $\sim$0.3333; and the rotation number should exhibit a flat region at this value. (Note that only every third value of the phase $\phi(n)$ is used for our analytical calculation of γ_{13} using Eq. 5.)

In the top panel of Fig. 11, synchronization index γ_{13} (solid line) and the rotation number (dashed line) are shown as a function of ρ , with a small amount of noise added to the system ($D = 6 \times 10^{-6}$). The rotation number shows a flat region for 0.33333, as expected, and the synchronization index shows a nearly uniform peak (actually it is equal to its maximal value of unity) over the length of the locking region. As noise is increased, secondary peaks appear (middle panel, $D = 6 \times 10^{-5}$). When the noise is increased again, the γ_{13} peak breaks up further (bottom panel, $D = 8 \times 10^{-5}$). Note also how the flat region of the rotation number appears smeared out as the noise is increased; this "smearing" is also a factor in our experimental data, where sharp peaks in the synchronization index are often observed in the absence of a clearly defined flat region in the frequency-detuning curve.

In the circle map model, the breakup of the γ_{13} peak as noise increases is likely due to the following. In the 1:3 locking region, the probability density of the phases will have three peaks. In order to calculate γ_{13}, one must take every third phase value; when noise is minimal, this is equivalent to landing on the same one of the three peaks each time, generating a measure of the intensity of the first Fourier mode of this peak. When noise is added, however, one will occasionally land on other peaks, leading to dips in the calculated intensity of the chosen peak of interest (the one we

"intend" to land on by selecting every third point). At high noise levels, there will be significant variations in the measured intensity of the peak of interest from one value of ρ to another, giving rise to the appearance of hills and valleys in the middle and bottom panels of Fig. 11. As the number of iterates at each value of ρ is increased toward infinity at a given noise level, these differences should be smoothed out (note that in this case 40,000 iterates of the circle map are calculated at each value of ρ and the first 20,000 transients). Such smoothing, however, is not attainable for data sets of reasonable experimental length, such as shown in Fig. 5.

4.4 The observation of stochastic synchronization; relation to stochastic resonance

Based on the frequency-detuning curves and synchronization index, it is shown that stochastic synchronization does occur between the caudal photoreceptor and a periodic mechanical stimulus, suggesting that synchronization is the mode by which mechanical signals are transduced in this system. Synchronization index maxima are seen to shift to higher frequencies in the light, *indicating a change in the frequency response characteristics of the photoreceptor in the presence of light*.

While there is no overall increase in synchronization indices in the light (Table 1), an increase in γ_{11} does occur when the SNR of an applied stimulus is increased in the presence of light (Fig. 7; Bahar et al. 2002). The occurrence of a maximal synchronization index as input noise is increased is to be expected for a stochastic resonance effect. In general, it is expected that as the SNR of a weak periodic input increases, synchronization between the measured variable (neural spikes in this case) and the weak periodic input will increase (Neiman et al. 1998; Neiman et al. 1999c). The observations reported here are consistent with this prediction.

Pei et al. (1996) have reviewed various possible mechanisms for enhancement of the SNR by light. These authors considered whether light increases the gain in the CPRs of an input signal from the mechanoreceptors. However, a large proportion of the intrinsic variability in the CPR firing is believed to originate with hydrodynamic fluctuations of the mechanoreceptive hairs. Thus a putative gain mechanism should turn up the gain on both a periodic mechanical input and on random hydrodynamic noise. This is *not* observed experimentally, however. Background noise at the stimulus frequency does not increase proportionally to the power spectral peak of the periodic input. Pei et al. also considered a second mechanism in which light-triggered depolarization of the CPRs leads to a lowering of the firing threshold. However, a computational model based on this model was inconsistent with experimental data.

Pei et al. concluded that the most likely explanation for the observed stochastic-resonance-like effect was that light increased input noise in the CPR dendrites. The phase synchronization study presented here is consistent with this hypothesis. However, the biochemical effects of light on ion channel activity in the CPR dendrites, where the light response originates (Wilkens and Larimer 1972), are not well understood. Despite recent work on the biochemical origin of light sensitivity in the CPRs (Kruszewska and Larimer 1993), the issue remains far from resolved. A mechanism by which light adds internal noise to a synaptic input to the CPR has not yet been proposed.

4.5 Intrinsic neural oscillator

The observation of stochastic synchronization in the photoreceptor demonstrates that there is an intrinsic dynamical oscillator in the photoreceptor system whose frequency is altered by the presence of light. This means that the spikes recorded in the CPR axons are not driven exclusively by noise but at least in part by an intrinsic firing rate of the cell, though this is certainly modulated by noisy input from the nerve roots. Indeed, frequency locking as the driving frequency f_o is changed *cannot* occur without the presence of an intrinsic oscillator in the driven system (Pikovsky et al. 2001; Rosenblum et al. 2001). This interpretation of the CPR as a noisy oscillator is consistent with previous interpretations of this system in the literature (Wilkens 1988).

4.6 Relation of stochastic synchronization to neural coding

While the results shown here indicate that stochastic synchronization does occur between CPR firing and an applied periodic stimulus, the relation between this "coding" mechanism and "perception" by the crayfish remains problematic. A very significant issue is that the synchronization index calculated here is a measure inaccessible to the crayfish itself. An experimenter has access both to CPR spikes and to the periodic applied stimulus and has sufficient information needed to calculate phase relationships between the spike and the stimulus. In contrast, the crayfish can "see" only its own spikes. While in principle the stimulus frequency can be extracted from the spike train (via a peak in the power spectrum), it is not apparent how the crayfish could "calculate" a power spectrum from its own spikes. Even were such a calculation possible, the power spectrum does not preserve any information about the *phase relation* between the stimulus and the spikes. Thus synchronization indices are inaccessible to the crayfish.

A possible comparative coding mechanism, synchronization *between* the firing of the two CPRs, does not appear to be used by the crayfish, as indicated by the results in Fig. 10. While synchronization between the two photoreceptors does occur in both dark (top panels) and light (bottom panels), a K-S test shows no significant *difference between* in the distributions in dark and light. Thus it can be presumed that a change in inter-

CPR synchronization does not provide the crayfish with a comparative test for the presence of light.

What aspects of the results shown here, then, might actually be "seen" or "used" by the crayfish? Is it useful to know that periodic signals are encoded by stochastic synchronization when the crayfish itself cannot quantify this encoding? In fact, the role of stochastic synchronization may be quite significant. It suggests the possibility of statistical encoding of an external stimulus in environments too noisy for more careful spike timing precision. As an alternative encoding mechanism, closely related to the idea of spike timing precision but adapted to highly noisy environments, stochastic synchronization may be a powerful sensory-encoding technique employed by a variety of different types of animals in the detection of periodic signals against a highly variable sensory background.

Acknowledgements. This work was supported by Office of Naval Research grant N00014-96-1-1107 (Dr. Frank Moss, Prinicpal Investigator), and by an NIH/NINDS National Research Service Award to the author. The author would like to gratefully acknowledge many illuminating discussions with Drs. Frank Moss, Alexander Neiman, Lon A. Wilkens and David F. Russell, and to thank them for a critical reading of the manuscript. Many thanks also to Prof. Jürgen Kurths for a very useful discussion.

References

Bahar S, Neiman A, Wilkens LA, Moss F (2002) Phase synchronization and stochastic resonance effects in the crayfish caudal photoreceptor. Phys Rev E (Rapid Commun) 65: 050901

Bainbridge R (1958) The speed of swimming of fish as related to size and to the frequency and amplitude of the tail beat. J Exp Biol 35: 109–133

Bialek W, Rieke F, de Ruyter van Steveninck RR, Warland D (1991) Reading a neural code. Science 252: 1854–1857

Bleckmann H, Breithaupt T, Blickhan R, Tautz J (1991) The time course and frequency content of hydrodynamic events caused by moving fish, frogs and crustaceans. J Comp Physiol A 168: 749–757

Bruno MS, Kennedy D (1962) Spectral sensitivity of photoreceptor neurons in the sixth ganglion of the crayfish. Comp Biochem Physiol 6: 41–46

Dolan KT, Neiman A (2002) Surrogate analysis of coherent multichannel data. Phys Rev E 65: 026108

Douglass JK, Wilkens LA (1998) Directional selectivities of near-field filiform hair mechanoreceptors on the crayfish tailfan (Crustacea: Decapoda). J Comp Physiol A 183: 23–34

Drucker EG, Jensen JS (1996a) Pectoral fin locomotion in the striped surfperch. I. Kinematic effects of swimming speed and body size. J Exp Biol 199: 2235–2242

Drucker EG, Jensen JS (1996b) Pectoral fin locomotion in the striped surfperch. II. Scaling swimming kinematics and performance at a gait transition. J Exp Biol 199: 2243–2252

Edwards DH (1984) Crayfish extraretinal photoreception. I. Behavioral and motoneural responses to abdominal illumination. J Exp Biol 109: 291–306

Edwards DH, Heitler WJ, Krasne FB (1999) Fifty years of a command neuron: the neurobiology of escape behavior in the crayfish. Trends Neurosci 22(4): 153–161

Ellerby DJ, Altringham JD (2001) Spatial variation in fast muscle function of the rainbow trout Oncorhynchus mykiss during fast-starts and sprinting. J Exp Biol 204: 2239–2250

Flood PM, Wilkens LA (1978) Directional sensitivity in a crayfish mechanoreceptive interneurone: analysis by root ablation. J Exp Biol 77: 89–106

Goodall C, Chapman C, Neil D (1990) The acoustic response threshold of the Norway lobster, *Nephrops norvegicus*, in a free sound field. In: Wiese K, Krenz WD, Tautz J, Reichert H, Mulloney B (eds) Frontiers in crustacean neurobiology. Birkhäuser, Basel, pp 106–113

Heberholz J, Issa FA, Edwards DH (2001) Patterns of neural circuit activation and behavior during dominance hierarchy formation in freely behaving crayfish. J Neurosci 21(8): 2759–2767

Hunter JD, Milton JG, Thomas PJ, Cowan JD (1998) Resonance effect for neural spike time reliability. J Neurophysiol 80(3): 1427–1438

Huygens C (1673) Horoloqium Oscilatorium. Parisiis, France

Kennedy D (1958a) Responses from the crayfish caudal photoreceptor. Am J Opthal 46: 19–26

Kennedy D (1958b) Electrical activity of a 'primitive' photoreceptor. Ann NY Acad Sci 74: 329–336

Kennedy D (1963) Physiology of photoreceptor neurons in the abdominal nerve cord of the crayfish. J Gen Physiol 46: 551–572

Krasne FB, Lee SC (1988) Response-dedicated trigger neurons as control points for behavioral actions: selective inhibition of lateral giant command neurons during feeding in the crayfish. J Neurosci 8(10): 3703–3712

Kruszewska B, Larimer JL (1993) Specific second messengers activate the caudal photoreceptor of the crayfish. Brain Res 618: 32–40

Moon FC (1992) Chaotic and fractal dynamics: an introduction for scientists and engineers. Wiley, New York

Neiman A (1994) Synchronization-like phenomena in coupled stochastic bistable systems. Phys Rev E 49: 3484–3487

Neiman A, Feudel U, Kurths J (1995) The cumulant approach for investigating the noise influence on model-locking bifurcations. J Phys A Math Gen 28: 2471–2480

Neiman A, Silchenko A, Anishchenko V, Schimansky-Geier L (1998) Stochastic resonance: noise-induced phase coherence. Phys Rev E 58(6): 7118–7125

Neiman A, Schimansky-Geier L, Cornell-Bell A, Moss F (1999a) Noise-enhanced phase synchronization in excitable media. Phys Rev Lett 83(23): 4896–4899

Neiman A, Pei X, Russell D, Wojtenek W, Wilkens LA, Moss F, Braun HA, Huber MT, Voigt K (1999b) Synchronization of the noisy electrosensitive cells in the paddlefish. Phys Rev Lett 82(3): 660–663

Neiman A, Schimansky-Geier L, Moss F, Shulgin B, Collins JJ (1999c) Synchronization of noisy systems by stochastic signals. Phys Rev E 60(1): 284–292

Neiman A, Russell DF, Pei X, Wojtenek W, Twitty J, Simonotto E, Wettring BA, Wagner E, Wilkens LA, Moss F (2000) Stochastic synchronization of electroreceptors in the paddlefish. Int J Bifurc Chaos 10: 2499–2517

Pei X, Wilkens LA, Moss F (1996a) Light enhances hydrodynamic signaling in the multimodal caudal photoreceptor interneurons of the crayfish. J Neurophysiol 76(5): 3002–3011

Pei X, Wilkens LA, Moss F (1996b) Noise-mediated spike timing precision from aperiodic stimuli in an array of Hodgkin-Huxley-type neurons. Phys Rev Lett 77: 4679–4682

Pikovsky A, Rosenblum M, Kurths J (2001) Synchronization: a universal concept in nonlinear sciences. Cambridge University Press, Cambridge, UK

Plummer MR, Tautz J, Wine JJ (1986) Frequency coding of waterborne vibrations by abdominal mechanosensory neurons in the crayfish *Procambarus clarkii*. J Comp Physiol A Sens Neural Behav Physiol 158: 751–764

Popper AN, Salmon NM, Horch KW (2001) Acoustic detection and communication by decapod crustaceans. J Comp Physiol A 187: 83–89

Rosenblum MG, Pikovsky AS, Kurths J (1996) Phase synchronization of chaotic oscillators. Phys Rev Lett 76: 1804–1807

Rosenblum MG, Pikovsky AS, Schäfer C, Tass P, Kurths J (2001) Phase synchronization: from theory to data analysis. In: Moss F, Gielen S (eds) Handbook of biological physics. Neuroinformatics, vol 4, Ch. 9. Elsevier, pp 279–321

Schäfer C, Rosenblum MG, Kurths J (1998a) Heartbeat synchronized with ventilation. Nature 392: 239–240

Schäfer C, Rosenblum MG, Abel H, Kurths J (1998b) Synchronization in the human cardiorespiratory system. Phys Rev E 60: 857–870

Simon TW, Edwards DH (1990) Light-evoked walking in crayfish: behavioral and neuronal responses triggered by the caudal photoreceptor. J Comp Physiol A Sens Neural Behav Physiol 166: 745–755

Sokal RR, Rohlf FJ (1981) Biometry. Freeman, San Francisco Second edition.

Stratonovich RL (1967) Topics in the theory of random noise, vol 2. Gordon and Breach, New York

Steuer R, Ebeling W, Russell DF, Bahar S, Neiman A, Moss F (2001) Entropy and local uncertainty of data from sensory neurons. Phys Rev E 64: 061911

Tass P, Rosenblum MG, Weule J, Kurths J, Pikovsky AS, Volkmann J, Schnitzler A, Freund J-H (1998) Detection of n:m phase-locking from noisy data: application to magnetoencephalography. Phys Rev Lett 81: 3291–3294

van Harreveld A (1936) A physiological solution for fresh-water crustacea. Proc Soc Exp Biol 34: 428–432

Webb PW (2002) Kinematics of plaice, Pleuronectes platessa, and cod, Gadus porhua, swimming near the bottom. J Exp Biol 205(14): 2125–2134

Welsh JH (1934) The caudal photoreceptor and responses of the crayfish to light. J Cell Comp Physiol 4: 379–388

Wiese K (1976) Mechanoreceptors for near-field water displacements in crayfish. J Neurophysiol 39(4): 816–833

Wiese K, Calabrese RL, Kennedy D (1976) Integration of directional mechanosensory input by crayfish interneurons. J Neurophysiol 39(4): 834–843

Wiesenfeld K, Moss F (1995) Stochastic resonance: from ice ages to crayfish and squids. Nature 373: 33–36

Wilkens LA, Larimer JL (1972) The CNS photoreceptor of the crayfish: morphology and synaptic activity. J Comp Phyisol 80: 389–407

Wilkens LA (1988) The crayfish caudal photoreceptor: advances and questions after the first half century. Comp Biochem Physiol 91C(1): 61–68

Wilkens LA, Douglass JK (1994) A stimulus paradigm for analysis of near-field hydrodynamics sensitivity in crustaceans. J Exp Biol 189: 263–272